PASSIVE CONTROL OF MAGNETO-NANOMATERIALS TRANSIENT FLOW SUBJECT TO NON-LINEAR THERMAL RADIATION

by

Ikram ULLAH[a*], Syed Irfan SHAH[b], Gul ZAMAN[c], Taseer MUHAMMAD[d,e], and Zakir HUSSAIN[f]

[a] Department of Sciences and Humanities,
National University of Computer and Emerging Sciences, Peshawar (KPK), Pakistan
[b] Department of Sciences and Humanities,
National University of Computer and Emerging Sciences, Islamabad, Pakistan
[c] Department of Mathematics, University of Malakand Chakdara,
Lower Dir (KPK), Pakistan
[d] Department of Mathematics, College of Sciences, King Khalid University,
Abha, Saudi Arabia
[e] Mathematical Modelling and Applied Computation Research Group (MMAC),
Department of Mathematics, King Abdulaziz University, Jeddah, Saudi Arabia
[f] Department of Mathematics, University of Baltistan, Skardu, Pakistan

Original scientific paper
https://doi.org/10.2298/TSCI201015169U

Present investigation is concerned with mixed convection flow of Williamson nanoliquid over an unsteady slandering stretching sheet. Aspects of non-linear thermal radiation, Brownian diffusion, and thermophoresis effects are addressed. Non-linear stretching surface of varying thickness induce the flow. Novel features of combined zero mass flux and convective conditions are accounted. Use of appropriate transformations results into the non-linear ODE. Computations for the convergent solutions are provided. Graphs are designed for interpretations to quantities. Nusselt number and surface drag are computationally inspected. Our computed results indicate that attributes of nanoparticles and non-linear thermal radiation enhance the temperature distribution.

Key words: *natural and force convection, zero mass flux condition, nanoparticles, non-linear thermal radiation*

Introduction

Nanomaterials are developed by utilization of tiny less nanometer particles into traditional liquids like water, ethylene glycol and oils. Choi and Eastman [1] firstly illustrated this novel kind of materials known as nanomaterials. These nanometers particles have remarkable physical and chemical characteristics. Such characteristics has motivated several researchers [2-6] to explore the aspects of heat transportation via nanomaterials. They noticed that occurrence of nanoparticles in liquids upsurges crucially the liquid thermal conductance and subsequently ameliorate heat transport properties. Besides this, numerous researchers have recently investigated different convective flow problems regarding nanomaterials, [7, 8]. Buongiorno [2] and Tiwari and Das [3] presented a detailed review regarding convective heat

* Corresponding author, e-mail: ikram020@yahoo.com

transport in nanoliquids. Buongiorno [2] perceived that absolute velocity of nanoparticles can be considered as the addition of base liquid and relative velocities. However, the model given by Tiwari and Das [3] explores response of nanoliquids taking into interpretation the solid volume fraction of nanoliquid. Here we analyze the flow and heat transport features for targeted problem utilizing the model given by Buongiorno [2]. Recently this model has been utilized by several researchers considering different flow situations [9-14].

Solar radiation is the non-polluting and non-conventional inception of energy. Actually this is obtained from radiant light and sun. Recent technology and modern science are greatly compelled towards solar radiation due to its extensive utilizations in photovoltaic cells, solar heating, artificial photosynthesis, solar electricity, *etc.* The small size of nanoparticles in nanomaterials consumes radiation extensively with that of de Broglie wavelength. Thus nanoparticles also declare the favorable quality of ameliorating radiative characteristics of liquids [15]. Few attempts regarding solar radiation can be consulted through [16-18] and several attempts therein. On the other hand the simultaneous natural/forced convective flow (mixed convection flow) has been reported experimentally, analytically and numerically [19-22]. This sort of flow is especially appealing owing to its importance in numerous engineering and industrial utilizations like electronic cooling, chemical process, solar systems, liquid storage tanks, nuclear power technology, *etc.*

Considerable research have been carried out by the researchers for the analysis of laminar flow by moving surface owing to its ever growing industrial utilizations in condensation process, glass and polymer industries, cooling procedure of metallic plate in cooling bath, and plastic sheets discharge. Sakiadis [23] led the basis for the stretched flow problem. Extensive analyses covering numerical and analytical investigations interpreting diverse characteristics of stretched flow are made [24-26]. Surface with varying thickness finds demand in nuclear reactor technology, acoustical components, machine design, architecture, naval structures, *etc.* The idea of varying thickness sheet initiated all the way through linearly deforming materials like nozzles and needles. Lee [27] initiated the idea of varying thickness. Afterwards other researchers [28-31] considered flow features by slendering sheet.

The novelty of current article is to explore the aspects of non-linear thermal radiation and mixed convection in unsteady flow of Williamson nanofluid bounded by unsteady slendering sheet. Energy and concentration expressions are characterized through Brownian motion and thermophoresis phenomena. Implementation of homotopic scheme [32-34] help us to analyze governing mathematical problems. Plots have been interpreted to examine the characteristics of key variables. Representation of skin friction and Nusselt number have been numerically examined.

Problems development

Here mathematical formulation for unsteady mixed convection 2-D flow of Williamson liquid stretching sheet of variable thickness, $y = \delta(x + b)^{(1-n)/2}$, δ being small, is given. Let $u = U_0[(x+b)^n/(1-\gamma_1 t)]$ declares the sheet velocity, fig. 1. Further keep in mind that $n = 1$ corresponds to flat stretching surface. Buoyancy force effects are considered. Energy expression is radiation and convective surface condition. Novel aspects of zero mass flux condition is also taken at the surface. The aspects of thermophoretic and Brownian diffusions are accounted. Ambient and sheet fluid concentrations and temperatures are symbolized by (C_w, T_f) and (C_∞, T_∞) respectively. The resulting boundary layer problems are defined by [10, 35-37]:

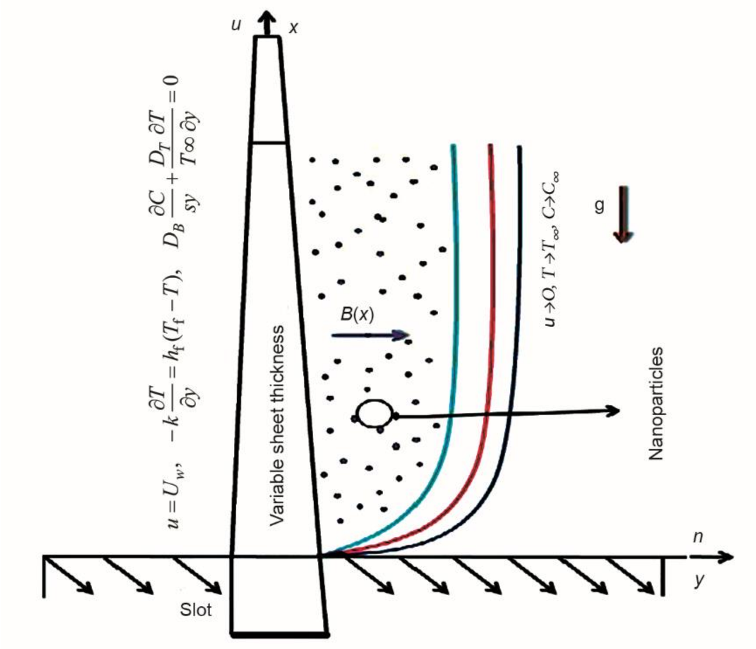

Figure 1. Flow geometry

$$\frac{\partial u}{\partial x}+\frac{\partial v}{\partial y}=0 \tag{1}$$

$$\frac{\partial u}{\partial t}+u\frac{\partial u}{\partial x}+v\frac{\partial u}{\partial y}=\nu\frac{\partial^2 u}{\partial y^2}+2\nu\Gamma\frac{\partial u}{\partial y}\left(\frac{\partial^2 u}{\partial y^2}\right)+\mathrm{g}\beta_{\mathrm{T}}(T-T_\infty)+\mathrm{g}\beta_{\mathrm{C}}(C-C_\infty) \tag{2}$$

$$\frac{\partial T}{\partial t}+u\frac{\partial T}{\partial x}+v\frac{\partial T}{\partial y}=\alpha_m\frac{\partial^2 T}{\partial y}+\frac{(\rho c)_p}{(\rho c)_f}\left[D_B\frac{\partial T}{\partial y}\frac{\partial C}{\partial y}+\frac{D_{\mathrm{T}}}{T_\infty}\left(\frac{\partial T}{\partial y}\right)^2\right]-\frac{1}{(\rho c)_f}\frac{\partial q_{\mathrm{r}}}{\partial y} \tag{3}$$

$$\frac{\partial C}{\partial t}+u\frac{\partial C}{\partial x}+v\frac{\partial C}{\partial y}=\left(\frac{D_{\mathrm{T}}}{T_\infty}\right)\frac{\partial^2 T}{\partial y^2}+D_B\frac{\partial^2 C}{\partial y^2} \tag{4}$$

with

$$\begin{gathered}u=U_w(x,t)=\frac{(x+b)^n}{(1-\gamma_1 t)}U_0, \quad v(x,t)=0, \quad -k\frac{\partial T}{\partial y}=h_f(T_f-T)\\ D_B\frac{\partial C}{\partial y}+\frac{D_T}{T_\infty}\frac{\partial T}{\partial y}=0 \text{ at } y=\delta(x+b)^{\frac{1-n}{2}}\end{gathered} \tag{5}$$

$$u\to 0, \quad T\to T_\infty, \quad C\to C_\infty \text{ as } y\to\infty \tag{6}$$

where (u, v) denotes the liquid velocities in direction of x- and y-axis, b and γ_1 – the rate constants with $b>0$ and $\gamma_1 \geq 0$, Γ – the time constant, g – the gravitational acceleration, μ_0 –

the dynamic viscosity, h_f – the coefficient of heat transport, ρ_f – the density of liquid, β_T and β_C – the coefficient of (thermal, solutal) expansions, T and T_0 stand for liquid and reference temperatures, n – the velocity power index, $(\rho c)_f$, $(\rho c)_p$ – the liquid and nanoparticles capacities, q_r – the radiative heat flux, D_B – the diffusion coefficient, C_0, and C – the reference and fluid concentrations, ν – the kinematic viscosity, $\alpha_m = k/(\rho c)_f$ for the thermal diffusivity, and D_T – the coefficient of thermophoretic diffusion.

The radiative heat flux q_r estimation is:

$$q_\mathrm{r} = -\frac{4\sigma^{**}}{3m^{**}}\frac{\partial(T^4)}{\partial y} = -\frac{16\sigma^{**}T^3}{3m^{**}}\frac{\partial T}{\partial y} \tag{7}$$

where σ^{**} designates the Stefan-Boltzman and m^{**} symbolized the coefficient of mean absorption. Upon using eq. (7), the energy expression becomes:

$$u\frac{\partial T}{\partial x} + v\frac{\partial T}{\partial y} = \alpha_m \frac{\partial^2 T}{\partial y^2} + \frac{(\rho c)_p}{(\rho c)_f}\left[D_B \frac{\partial T}{\partial y}\frac{\partial C}{\partial y} + \frac{D_\mathrm{T}}{T_\infty}\left(\frac{\partial T}{\partial y}\right)^2\right] - \frac{1}{(\rho c_p)}\frac{\partial}{\partial y}\left(\frac{16\sigma^{**}T^3}{3m^{**}}\frac{\partial T}{\partial y}\right) \tag{8}$$

By invoking the following transformations:

$$\begin{gathered} u = U_0\frac{(x+b)^n}{1-\gamma_1 t}F'(\eta), \quad v = -\sqrt{\frac{n+1}{2}\nu U_0\frac{(x+b)^{n-1}}{1-\gamma_1 t}}\left[F(\eta) + \eta F'(\eta)\frac{n-1}{n+1}\right] \\ \eta = y\sqrt{\frac{n+1}{2}\frac{U_0(x+b)^{n-1}}{\nu(1-\gamma_1 t)}}, \quad \Theta(\eta) = \frac{T-T_\infty}{T_f - T_\infty}, \quad \Phi(\eta) = \frac{C-C_\infty}{C_\infty} \end{gathered} \tag{9}$$

Equation (1) reduces trivially while other eqs. (2)-(6) and (8) are:

$$F''' + FF'' - \left(\frac{2n}{n+1}\right)F'^2 - \left(\frac{n}{n+1}\right)\left(\frac{\eta}{2}F'' + F'\right) + \sqrt{\frac{n+1}{2}}\mathrm{We}F''F''' + \lambda(\Theta + N\Phi) = 0 \tag{10}$$

$$\begin{gathered} \left(1 + \frac{4}{3}Rd\right) + \frac{4}{3}Rd[(\theta_w - 1)^3(3\Theta'^2\Theta'^2 + \Theta^3\Theta'') + 3(\theta_w - 1)^2(2\Theta'^2\Theta + \Theta^2\Theta'') + \\ +3(\theta_w - 1)(\Theta'^2 + \Theta\Theta'')] - \\ -\mathrm{Pr}\left[A\frac{n}{n+1}(\Theta + \eta\Theta') + \frac{1-n}{1+n}F'\Theta - F\Theta' - N_\mathrm{b}\Theta'\Phi' - N_t\Theta'^2\right] = 0 \end{gathered} \tag{11}$$

$$\Phi'' + \mathrm{Sc}\left[A\frac{n}{n+1}(\Phi + \eta\Phi') + \left(\frac{1-n}{1+n}\right)F'\Phi - F\Phi'\right] + \left(\frac{N_\mathrm{t}}{N_\mathrm{b}}\right)\Theta'' = 0 \tag{12}$$

$$\begin{gathered} F(\alpha) = \alpha\frac{1-n}{1+n}, \quad F'(\alpha) = 1, \quad F'(\infty) \to 0 \\ \Theta'(\alpha) = -\gamma[1 - \Theta(\alpha)], \quad \Phi'(\alpha) + \frac{N_\mathrm{t}}{N_\mathrm{b}}\Theta'(\alpha) = 0 \\ \Theta(\infty) \to 0, \quad \Phi(\infty) \to 0 \end{gathered} \tag{13}$$

where

$$\alpha = \delta\sqrt{\frac{n+1}{2}\frac{U_0}{\nu}}$$

designates wall thickness parameter and:

$$\alpha = \eta = \delta\sqrt{\frac{n+1}{2}\frac{U_0}{\nu}}$$

Considering

$$F(\eta) = f(\eta-\alpha) = f(\xi),\ \ \Theta(\eta) = \theta(\eta-\alpha) = \theta(\xi),\ \ \Phi(\eta) = \phi(\eta-\alpha) = \phi(\xi) \tag{14}$$

Equation (8) and eqs. (10)-(13) yield:

$$f''' + ff'' - \left(\frac{2n}{n+1}\right)f'^2 - \left(\frac{n}{n+1}\right)\left(\frac{\xi}{2}f'' + f'\right) + \sqrt{\frac{n+1}{2}}\mathrm{We}f''f''' + \lambda(\theta + N\phi) = 0 \tag{15}$$

$$\left(1+\frac{4}{3}Rd\right) + \frac{4}{3}Rd[(\theta_w-1)^3(3\theta'^2\theta^2 + \theta^3\theta'') + 3(\theta_w-1)^2(2\theta'^2\theta + \theta^2\theta'') +$$
$$+3(\theta_w-1)(\theta'^2 + \theta\theta'')] -$$
$$-\mathrm{Pr}\left[A\frac{n}{1+n}(\theta + \xi\theta') + \frac{1-n}{1+n}f'\theta - f\theta' - N_\mathrm{b}\theta'\phi' - N_\mathrm{t}\theta'^2\right] = 0 \tag{16}$$

$$\phi'' + \mathrm{Sc}\left[A\frac{n}{n+1}(\phi + \xi\phi') + \frac{1-n}{1+n}f'\phi - f\phi'\right] + \frac{N_\mathrm{t}}{N_\mathrm{b}}\theta'' = 0 \tag{17}$$

$$f(0) = \alpha\frac{1-n}{1+n},\quad f'(0) = 1,\quad f'(\infty) \to 0$$
$$\theta'(0) = -\gamma[1-\theta(0)],\quad \phi'(0) + \frac{N_\mathrm{t}}{N_\mathrm{b}}\theta'(0) = 0 \tag{18}$$
$$\theta(\infty) \to 0,\quad \phi(\infty) \to 0$$

where λ is the mixed convection variable, Pr – the Prandtl number, N – the buoyancy ratio, N_t – the thermophoresis variable, N_b – the Brownian motion variable, Sc – the Schmidt number, We – the Weissenberg number, θ_w – the temperature ratio parameter, A – the unsteadiness parameter, γ – the convective parameter, Re_x – the Reynolds number, and Rd – the radiation variable. These variables are:

$$A = \frac{\gamma_1(b+x)^{1-n}}{U_0},\quad \lambda = \frac{\mathrm{Gr}_x}{\mathrm{Re}_x^2},\quad \mathrm{Gr}_x = \frac{\mathrm{g}\beta_\mathrm{T}(T_f - T_\infty)(b+x)^3}{\nu^2},\quad \gamma = \frac{h_f}{k}\sqrt{\frac{2\nu(b+x)}{(n+1)U_w}}$$
$$N = \frac{\beta_C C}{\beta_\mathrm{T}(T_f - T_\infty)},\quad \mathrm{Pr} = \frac{\nu}{\alpha_m},\quad \mathrm{Sc} = \frac{\nu}{D_B},\quad N_b = \frac{(\rho c)_p}{(\rho c)_f}\frac{D_B C_\infty}{\nu} \tag{19}$$
$$N_\mathrm{t} = \frac{(\rho c)_p}{(\rho c)_f}\frac{D_\mathrm{T}(T_f - T_\infty)}{T_\infty\nu},\quad Rd = \frac{4\sigma^{**}T_\infty^3}{m^{**}k},\quad \mathrm{We} = \Gamma\frac{\sqrt{U_0^3(b+x)^{3n-1}}}{(1-\gamma_1 t)^3},\quad \mathrm{Re}_x = U_w\frac{b+x}{\nu}$$

The expressions of skin friction, C_{f_x}, and local heat flux rate at the surface, Nu_x, are:

$$C_{\mathrm{f}_x} = \frac{\tau_{yx}\,|_{y=\delta(b+x)^{\frac{1-n}{2}}}}{\frac{1}{2}\rho U_w^2}\,|= \frac{\mu_0\left[\frac{\partial u}{\partial y}+\frac{\Gamma}{2}\left(\frac{\partial u}{\partial y}\right)^2\right]_{y=\delta(b+x)^{\frac{1-n}{2}}}}{\rho U_w^2} \tag{20}$$

$$\mathrm{Nu}_x = (q_r)_w + \frac{(b+x)q_w\,|_{y=\delta(b+x)^{\frac{1-n}{2}}}}{D_B(T_f - T_\infty)} = -\frac{\left(\frac{\partial T}{\partial y}\right)_{y=\delta(b+x)^{\frac{1-n}{2}}}}{T_f - T_\infty} + (q_r)_w \tag{21}$$

In non-dimensional form we have:

$$(\mathrm{Re}_x)^{0.5} C_{f_x} = \sqrt{\frac{(n+1)}{2}}\, f''(0) + \frac{(n+1)}{4}\mathrm{We} f''^2(0) \tag{22}$$

$$(\mathrm{Re}_x)^{-0.5}\mathrm{Nu}_x = \sqrt{\left(\frac{n+1}{2}\right)}\left(1+\frac{4}{3}Rd\{1+(\theta_w-1)[\theta(0)]^3\}\right)\theta'(0) \tag{23}$$

Analysis of convergent solutions

We select initial guesses (f_0, θ_0, ϕ_0) and linear operators ($(\bar{\mathbf{L}}_f, \bar{\mathbf{L}}_\theta, \bar{\mathbf{L}}_\phi)$ in the forms:

$$\begin{aligned} f_0(\xi) &= \alpha\frac{1-n}{1+n} + 1 - \mathrm{e}^{-\xi} \\ \theta_0(\xi) &= \frac{\gamma}{1+\gamma}\mathrm{e}^{-\xi} \\ \phi_0(\xi) &= -\frac{\gamma}{1+\gamma}\frac{N_\mathrm{t}}{N_\mathrm{b}}e^{-\xi} \end{aligned} \tag{24}$$

with

$$\begin{aligned} \bar{\mathbf{L}}_f\left[D_1^{**} + D_2^{**}\mathrm{e}^{\xi} + D_3^{**}\mathrm{e}^{-\xi}\right] &= 0 \\ \bar{\mathbf{L}}_\theta\left[D_4^{**}\mathrm{e}^{\xi} + D_5^{**}\mathrm{e}^{-\xi}\right] &= 0 \\ \bar{\mathbf{L}}_\phi\left[D_6^{**}\mathrm{e}^{\xi} + D_7^{**}\mathrm{e}^{-\xi}\right] &= 0 \end{aligned} \tag{25}$$

where D_i^{**} (i = 1-7)declared arbitrary constants and have the following values:

$$\begin{gathered} D_2^{**} = D_4^{**} = D_6^{**} = 0, \quad D_3^{**} = \frac{\partial f_m^*(\xi)}{\partial \xi}\Big|_{\xi=0}, \quad D_1^{**} = -D_3^{**} - f_m^*(0) \\ D_5^{**} = \frac{1}{1+\gamma}\frac{\partial \theta_m^*(\xi)}{\partial \xi}\Big|_{\xi=0} - \frac{\gamma}{1+\gamma}\theta_m^*(0), \quad D_7^{**} = \frac{\partial \phi_m^*(\xi)}{\partial \xi}\Big|_{\xi=0} + \frac{N_\mathrm{t}}{N_\mathrm{b}}\left[\frac{\partial \theta_m^*(\xi)}{\partial \xi}\Big|_{\xi=0}\,\theta_m^*(0)\right] \end{gathered} \tag{26}$$

Homotopic scheme secure us regarding the convergence of approximate solutions. Here embedding variables $\hbar_f$, $\hbar_\theta$, and $\hbar_\phi$ have key role in convergence of derived solutions. Figures 2 and 3 indicated the $\hbar$-curves which enable us to pointed out the estimations for $\hbar_f$, $\hbar_\theta$, and $\hbar_\phi$. These acceptable ranges are $(-0.5 \le \hbar_f \le -1.5)$, $(-0.50 \le \hbar_\theta \le -1.84)$, and $(-0.20 \le \hbar_\phi \le -1.86)$. Moreover the convergence of HAM is inspected through tab. 1. It is noticed from tab. 1 that series solutions converge up to 35th order of estimations for velocity whereas 40th order of deformations are ample for the temperature and concentration distributions.

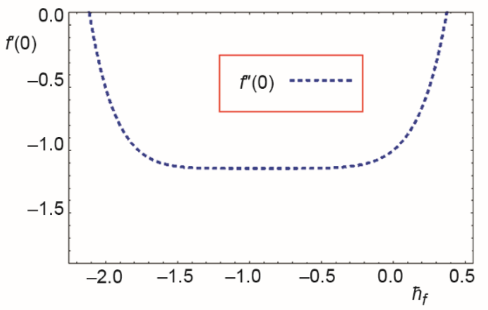

Figure 2. The $\hbar$-curve for f; α = 0.3, We = N = = Rd = 0.2 = γ = Nt, Nb = 0.5, Pr = 0.8 = Sc, A = 1.0, λ = 0.1, n = 0.9

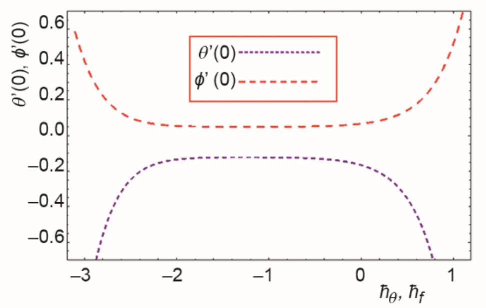

Figure 3. The $\hbar$-curve for $\theta(\xi)$ and $\phi(\xi)$; α = 0.3, We = N = Rd = 0.2 = γ = Nt, Nb = 0.5, Pr = 0.8 = Sc, A = 1.0, λ = 0.1, n = 0.9

Table 1. Convergence when Rd = N = 0.2 = We = γ = N_t, α = 0.3, A = 1.0 = θ_w, λ = 0.1, N_b = 0.5, Pr = 0.8 = Sc, and n = 0.9

Order of estimations	$-f''(0)$	$-\theta'(0)$	$\phi'(0)$
1	1.05802	0.15715	0.06286
10	1.14303	0.12665	0.05065
15	1.14399	0.12421	0.04968
20	1.14402	0.12419	0.04968
35	1.14403	0.12413	0.04958
40	1.14403	0.12412	0.04951
45	1.14403	0.12412	0.04951
50	1.14403	0.12412	0.04951
55	1.14403	0.12412	0.04951

Discussion

Features of various involved variables on $f'(\xi)$, $\theta(\xi)$, $\phi(\xi)$, $-(\mathrm{Re})^{1/2}C_{f_x}$, and Nu_x are investigated in this section. Such goal is achieved *via* figs. 4-21 and tabs. 2 and 3. Aspects of α on $f'(\xi)$ is depicted in fig. 4. Here decay in $f'(\xi)$ is remarked against α. Features of $f'(\xi)$ due to higher n is designed in fig. 5. Here velocity grows in response of higher n. Increase in n improves the surface velocity, which speed up liquid deformation. Behavior of $f'(\xi)$ *vs.* λ is interpreted in fig. 6. Clearly velocity rises *via* λ. Physically larger λ accompany a stronger buoyancy force and it leads to an increment in $f'(\xi)$. Velocity $f'(\xi)$ against N is exhibited in fig. 7.

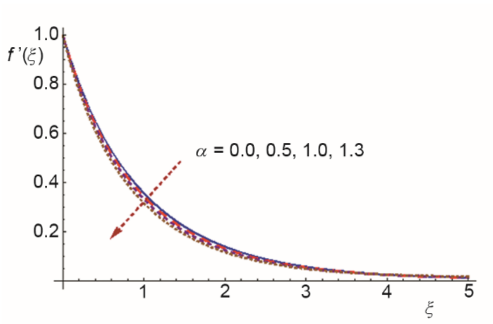

Figure 3. Response of $f'(\xi)$ against α; We = N = = Rd = 0.2 = γ = N_t, θ_w = 1.2, N_b = 0.5, Pr = 0.8 = Sc, A = 1.0, λ = 0.1, n = 0.9

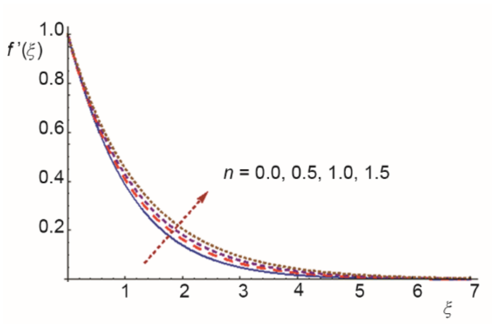

Figure 4. Response of $f'(\xi)$ against n; α = 0.3, We = N = Rd = 0.2 = γ = N_t, θ_w = 1.2, N_b = 0.5, Pr = 0.8 = Sc, A = 1.0, λ = 0.1

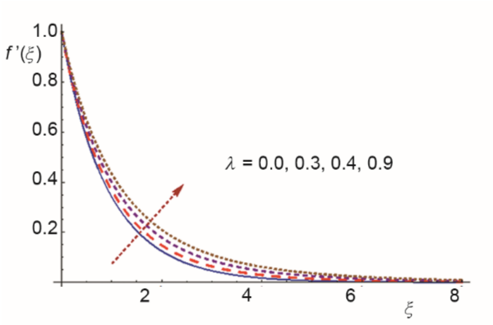

Figure 5. Response of $f'(\xi)$ against λ; α = 0.3, We = N = Rd = 0.2 = γ = N_t, θ_w = 1.2, N_b = 0.5, Pr = = 0.8 = Sc, A = 1.0, n = 0.9

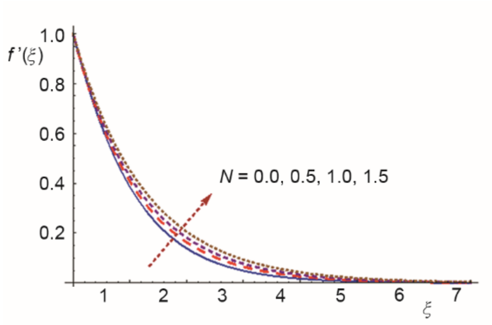

Figure 6. Response of $f'(\xi)$ against N; α = 0.3, We = 1.2, Rd = 0.2 = γ = N_t, θ_w = N_b = 0.5, Pr = 0.8 = Sc, A = 1.0, λ = 0.1, n = 0.9

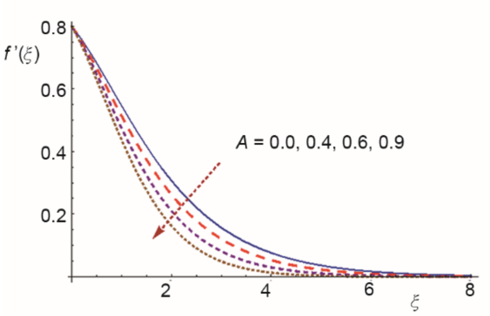

Figure 7. Response of $f'(\xi)$ against A; α = 0.3, We = N = Rd = 0.2 = γ = N_t, θ_w = 1.2, N_b = 0.5, Pr = 0.8 = Sc, λ = 0.1, n = 0.9

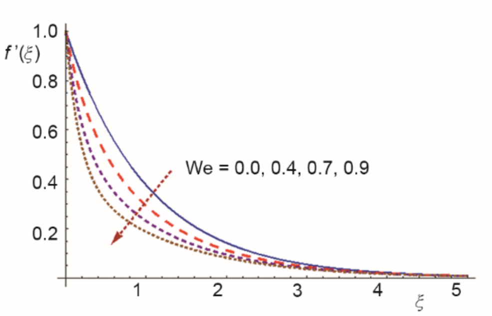

Figure 8. Response of $f'(\xi)$ against We; α = 0.3, N = Rd = 0.2 = γ = N_t, θ_w = 1.2, N_b = 0.5, Pr = 0.8 = Sc, A = 1.0, λ = 0.1, n = 0.9

Here $f'(\xi)$ grow up against N. Consequences of A on $f'(\xi)$ is depicted in fig. 8. For higher A the rate of stretching is smaller in x-direction which eventually diminish $f'(\xi)$. Effect of We on $f'(\xi)$ is shown in fig. 9. Larger We decays $f'(\xi)$. Aspects of α on $\theta(\xi)$ is presented in fig. 10. Here temperature field decays when α is enhanced. Variation of $\theta(\xi)$ via n is designated in

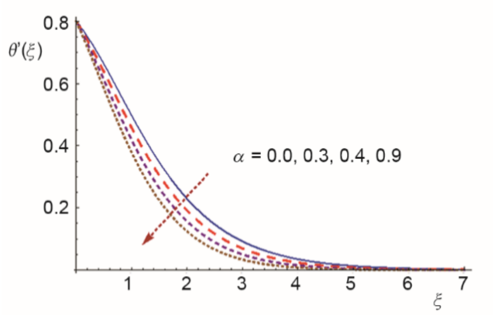

Figure 9. Response of $\theta(\xi)$ against α; We = N = Rd = 0.2 = γ = N_t, θ_w = 1.2, N_b = 0.5, Pr = 0.8 = Sc, A = 1.0, λ = 0.1, n = 0.9

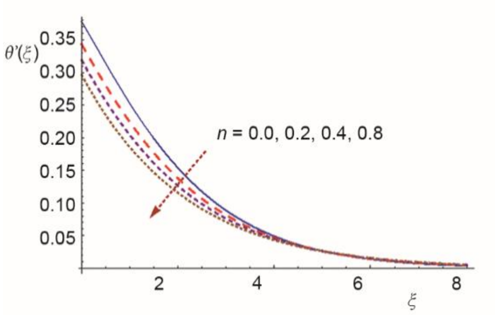

Figure 10. Response of $\theta(\xi)$ against n; α = 0.3, We = N = Rd = 0.2 = γ = N_t, θ_w = 1.2, N_b = 0.5, Pr = 0.8 = Sc, A = 1.0, λ = 0.1

fig. 11. Here temperature field enhances for larger n. Higher temperature $\theta(\xi)$ is liked with higher λ, fig. 12. In fact, higher λ leads to higher buoyancy forces which results in an increment of $\theta(\xi)$. Impact of N on $\theta(\xi)$ is explored through fig. 13. Here temperature is decreasing function of N. Physically N is the ratio of concentration to thermal buoyancy forces. Thus an enhancement in N corresponds to lower temperature. Remarkable features of $\theta(\xi)$ against N_t is displayed in fig. 14. It is inspected that $\theta(\xi)$ is boosted via N_t. It is because of the fact that in thermophoresis process, the heated liquid particles extracted towards cold regime from hot surface which corresponds to boosts up $\theta(\xi)$. Through fig. 15 the characteristics of Pr on temperature distribution is reported. For larger Pr the fluid temperature reduces. It is due to low rate of thermal diffusion which associates to larger Pr. It leads to reduction temperature. Figure 16 indicates influence of Rd on $\theta(\xi)$. It is noted that $\theta(\xi)$ increases when Rd enhances. It is important to remark that in radiation process, extra heat is added nanomaterials and thus temperature rises. Role of γ on $\theta(\xi)$ is pointed out in fig. 17. Here $\theta(\xi)$ rises for γ fig. 18 is displayed to examine the variation of N_t on $\phi(\xi)$. It is disclosed that $\phi(\xi)$ is lower for N_t. Effect of N_b on $\phi(\xi)$ is explored in fig. 19. Here $\phi(\xi)$ diminishes for N_t. The curves of concentration $\phi(\xi)$ for Sc are declared in fig. 20. Here it is inspected that grows in Sc decays concentration. Concentration is reduced via n, fig. 21. Numerical investigation of $-(\mathrm{Re})1/2C_{f_x}$ for involved variables of interest is executed in tab. 2. Here we pointed out that for increasing θ_w, n, A, and α, the skin friction is increased. Table 3 is prepared to explain features of quantities on Nu_x. It is noticed that Nu_x enhances for N, Rd, γ, N_t, N_b, and θ_w.

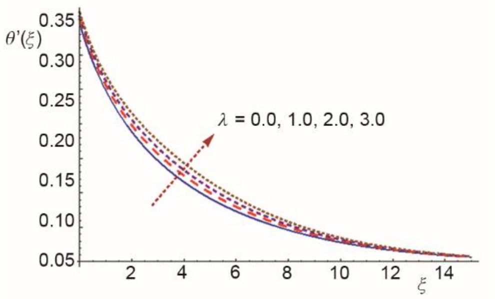

Figure 11. Response of $\theta(\xi)$ against λ; α = 0.3, We = N = Rd = 0.2 = γ = N_t, θ_w = 1.2, N_b = 0.5, Pr = 0.8 = Sc, A = 1.0, n = 0.9

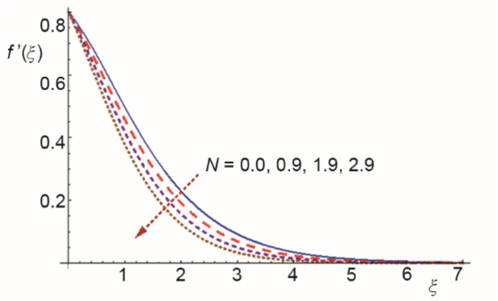

Figure 12. Response of $\theta(\xi)$ against N; α = 0.3, We = Rd = 0.2 = γ = N_t, θ_w = 1.2, N_b = 0.5, Pr = 0.8 = Sc, A = 1.0, λ = 0.1, n = 0.9

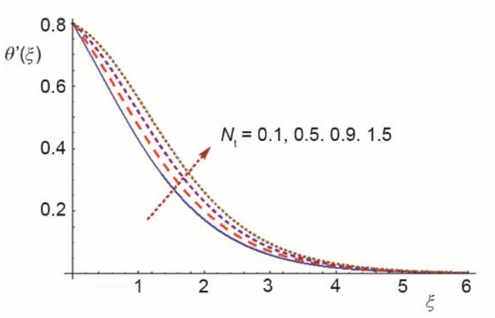

Figure 13. Response of $\theta(\xi)$ against N_t; $\alpha = 0.3$, We = N = Rd = 0.2 = γ = N_t, θ_w = 1.2, Pr = 0.8 = Sc, A = 1.0, λ = 0.1, n = 0.9

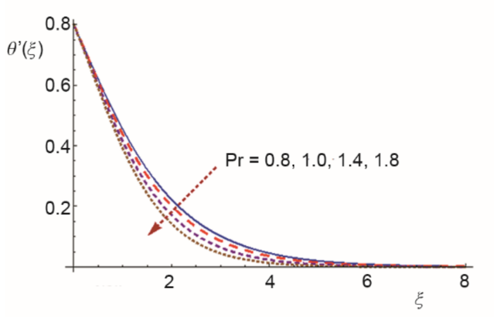

Figure 14. Response of $\theta(\xi)$ against Pr; $\alpha = 0.3$, We = N = Rd = 0.2 = γ = N_t, θ_w = 1.2, N_b = 0.5, Sc = 0.8, A = 1.0, λ = 0.1, n = 0.9

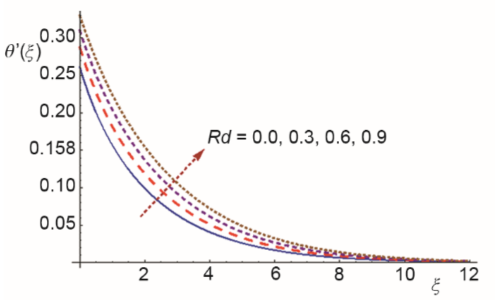

Figure 15. Response of $\theta(\xi)$ against Rd; $\alpha = 0.3$, We = N = 0.2 = γ = N_t, θ_w = 1.2, N_b = 0.5, Pr = 0.8 = Sc, A = 1.0, λ = 0.1, n = 0.9

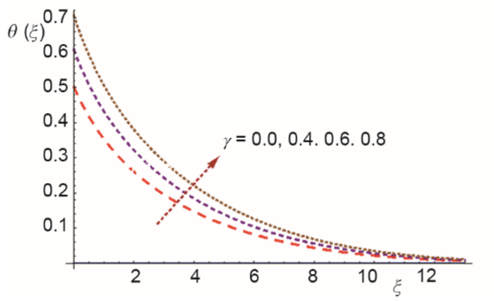

Figure 16. Response of $\theta(\xi)$ against γ; $\alpha = 0.3$, We = N = Rd = 0.2 = N_t, θ_w = 1.2, N_b = 0.5, Pr = 0.8 = Sc, A = 1.0, λ = 0.1, n = 0.9

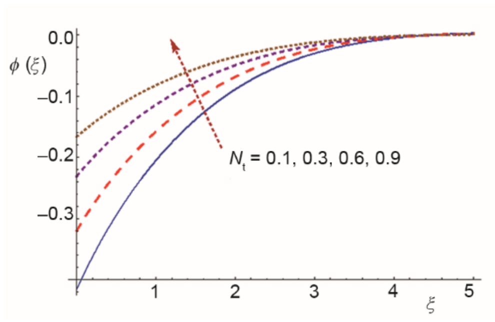

Figure 17. Response of $\phi(\xi)$ against N_t; $\alpha = 0.3$, We = N = Rd = 0.2 = γ, θ_w = 1.2, N_b = 0.5, Pr = 0.8 = = Sc, A = 1.0, λ = 0.1, n = 0.9

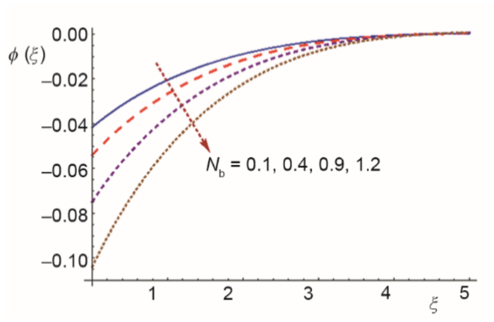

Figure 18. Response of $\phi(\xi)$ against N_b; $\alpha = 0.3$, We = N = Rd = 0.2 = γ = N_t, θ_w = 1.2, Pr = 0.8 = Sc, A = 1.0, λ = 0.1, n = 0.9

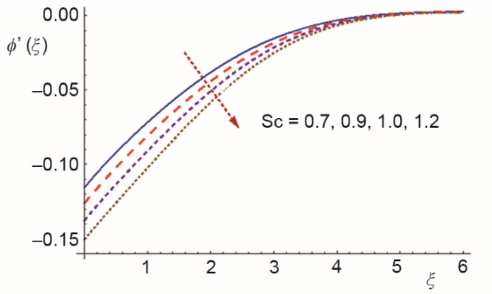

Figure 19. Response of ϕ (ξ) against Sc; α = 0.3, We = N = Rd = 0.2 = γ = N_t, θ_w = 1.2, N_b = 0.5, Pr = 0.8, A = 1.0, λ = 0.1, n = 0.9

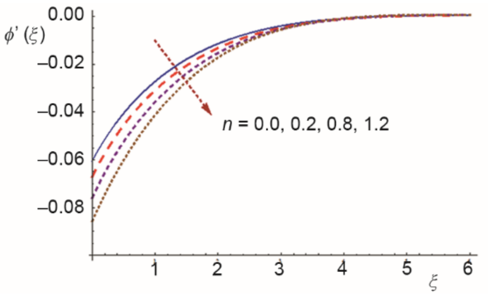

Figure 20. Response of ϕ (ξ) against n; α = 0.3, We = N = Rd = 0.2 = γ = N_t, θ_w = 1.2, N_b = 0.5, Pr = 0.8 = Sc, A = 1.0, λ = 0.1

Table 2. Numerical simulation for surface drag force $-(\mathrm{Re})^{0.5}C_{fx}$

Variable (fixed values)	Parameters		$-(\mathrm{Re})^{1/2}C_{fx}$
N = We = Rd = 0.2 = γ = N_t, α = 0.3, A = 1.0 = θ_w, λ = 0.1, N_b = 0.5, Pr = 0.8 = Sc	n	0.5	1.43310
		1.0	1.78509
		1.5	0.19674
N = Rd = 0.2 = γ = N_t, α = 0.3, A = 1.0 = θ_w, λ = 0.1, N_b = 0.5, Pr = 0.8 = Sc, n = 0.9	We	0.0	2.21832
		0.2	1.88636
		0.4	1.71881
N = We = Rd = 0.2 = γ = N_t, A = 1.0 = θ_w, λ = 0.1, N_b = 0.5, Pr = 0.8 = Sc, n = 0.9	α	0.0	1.70861
		0.3	1.72056
		0.6	1.73170
We = Rd = 0.2 = γ = N_t, α = 0.3, λ = 0.1, N_b = 0.5, Pr = 0.8 = Sc, n = 0.9	N	0.0	1.71622
		0.3	1.72107
		0.7	1.72707
N = We = Rd = 0.2 = γ = N_t, α = 0.3, θ_w = 1.0, A = 1.0 = θ_w, λ = 0.1, N_b = 0.5, Pr = 0.8 = Sc, n = 0.9	A	0.0	1.60630
		0.5	1.70459
		1.0	1.72056
N = We = Rd = 0.2 = γ = N_t, α = 0.3, A = 1.0, λ = 0.1, N_b = 0.5, Pr = 0.8 = Sc, n = 0.9	θ_w	0.5	1.23240
		1.0	1.24561
		1.5	1.28657
N = We = Rd = 0.2 = γ, α = 0.3, A = 1.0 = θ_w, λ = 0.1, N_b = 0.5, Pr = 0.8 = Sc, n = 0.9	N_t	0.1	1.71802
		0.3	1.72356
		0.5	1.73000
N = We = Rd = 0.2 = γ = N_t, α = 0.3, A = 1.0 = θ_w, λ = 0.1, Pr = 0.8 = Sc, n = 0.9	N_b	0.0	1.73435
		0.4	1.72138
		0.6	1.71939
N = We = Rd = 0.2 = N_t, α = 0.3, A = 1.0 = θ_w, λ = 0.1, N_b = 0.5, Pr = 0.8 = Sc, n = 0.9	γ	0.0	1.75820
		0.2	1.72090
		0.4	1.70660

Table 3. Numerical data of Nu_x

Variable (fixed values)	Parameters		$-\left(\frac{n+1}{2}\right)^{1/2}\theta'(0)$
N = We = Rd = 0.2 = N_t, α = 0.3, A = 1.0 = θ_w, λ = 0.1, N_b = 0.5, Pr = 0.8 = Sc	n	0.5	0.09808
		1.0	0.16103
		1.5	2.06351
N = Rd = 0.2 = γ = N_t, α = 0.3, A = 1.0 = θ_w, λ = 0.1, N_b = 0.5, Pr = 0.8 = Sc, n = 0.9	We	0.0	0.15243
		0.2	0.15327
		0.4	0.15636
N = We = Rd = 0.2 = γ = N_t, A = 1.0 = θ_w, λ = 0.1, N_b = 0.5, Pr = 0.8 = Sc, n = 0.9	α	0.0	0.15247
		0.3	0.15225
		0.6	0.15348
We = Rd = 0.2 = γ = N_t, α = 0.3, A = 1.0 = θ_w, λ = 0.1, N_b = 0.5, Pr = 0.8 = Sc, n = 0.9	N	0.0	0.15295
		0.3	0.15336
		0.7	0.15338
N = We = Rd = 0.2 = γ = N_t, α = 0.3, θ_w = 1.0, λ = 0.1, N_b = 0.5, Pr = 0.8 = Sc, n = 0.9	A	0.0	0.05466
		0.5	0.12733
		1.0	0.15225
N = We = Rd = 0.2 = γ = N_t, α = 0.3, A = 1.0, λ = 0.1, N_b = 0.5, Pr = 0.8 = Sc, n = 0.9	θ_w	0.5	0.13423
		1.0	0.17685
		1.5	0.19254
N = We = Rd = 0.2 = γ, α = 0.3, A = 1.0 = θ_w, λ = 0.1, N_b = 0.5, Pr = 0.8 = Sc, n = 0.9	N_t	0.1	0.15258
		0.3	0.15238
		0.5	0.15222
N = We = Rd = 0.2 = γ = N_t, α = 0.3, A = 1.0 = θ_w, λ = 0.1, Pr = 0.8 = Sc, n = 0.9	N_b	0.0	0.15301
		0.4	0.15225
		0.6	0.15242
N = We = Rd = 0.2 = N_t, α = 0.3, A = 1.0 = θ_w, λ = 0.1, N_b = 0.5, Pr = 0.8 = Sc, n = 0.9	γ	0.0	0.00000
		0.2	0.15211
		0.4	0.21916

Conclusions

In the current study we investigated non-linear thermal radiation in mixed convection flow of Williamson nanoliquid bounded by slendering stretching surface subjected to convective and zero mass flux conditions. The following points are as follows.

- Enhancement in unsteadiness parameter decays velocity.
- Velocity power index exhibits an opposite effect for velocity and temperature fields.
- Higher γ, λ, and Rd rises the temperature.

- Impact of N_b on $\phi(\xi)$ is qualitatively revers to that of N_t.
- Velocity and temperature fields are increasing function of mixed convection parameter λ.
- Skin friction and heat transfer coefficients are enhanced via unsteadiness variable and velocity power index.
- The HAM technique may use for different engineering problems and compared with solution obtained through different techniques [38-45].

Acknowledgment

The authors extend their appreciation to the Deanship of Scientific Research at King Khalid University, Abha, Saudi Arabia for funding this work through research groups program under grant number R.G.P-2/97/42.

References

[1] Choi, S. U. S., Eastman, J. A., Enhancing Thermal Conductivity of Fluids with Nanoparticles, *Proceedings*, ASME International Mechanical Engineering Congress and Exposition, San Francisco, Cal., USA, ASME, FED 231/MD, *66* (1995), pp. 99-105
[2] Buongiorno, J., Convective Transport in Nanofluids, *J. Heat Transfer Trans. ASME, 128* (2006), 3, pp. 240-250
[3] Tiwari, R. J., Das, M. K., Heat Transfer Augmentation in a Two-Sided Lid-Driven Differentially Heated Square Cavity Utilizing Nanofluids, *Int. J. Heat Mass Transfer, 50* (2007), 9-10, pp. 2002-2018
[4] Oztop, H. F., Abu-Nada, E., Numerical Study of Natural Convection in Partially Heated Rectangular Enclosures Filled with Nanofluids, *Int. J. Heat Fluid Flow, 29* (2008), 5, pp. 1326-1336
[5] Nield, D. A., Kuznetsov, A. V., The Cheng-Minkowycz Problem for Natural Convective Boundary-Layer Flow in a Porous Medium Saturated by a Nanofluid, *Int. J. Heat Mass Transfer, 52* (2009), 25-26, pp. 5792-5795
[6] Ullah, I., *et al.*, Dissipative Flow of Hybrid Nanoliquid (Aluminum Alloy Nanoparticles) with Nonlinear Thermal Radiation, *Physica Scripta, 94* (2019), 12, 125708
[7] Raza, J., *et al.*, Multiple Slip Effects on MHD Non-Newtonian Nanofluid flow Over a Non-Linear Permeable Elongated Sheet, Numerical and Statistical Analysis, *Multidiscipline Mod. Mat. Structures, 15* (2019), 5, pp. 913-931
[8] Hayat, T., *et al.*, Magnetohydrodynamic (MHD) Three-Dimensional Flow of Second Grade Nanofluid by a Convectively Heated Exponentially Stretching Surface, *J. Mol. Liq., 220* (2016), Aug., pp. 1004-1012
[9] Hsiao, K. L., Stagnation Electrical, MHD Nanofluid Mixed Convection with Slip Boundary on a Stretching Sheet, *Appl. Thermal Eng., 98* (2016), Apr., pp. 850-861
[10] Hayat, T., *et al.*, Flow of Magneto Williamson Nanoliquid Towards Stretching Sheet with Variable Thickness and Double Stratification, *Radiat. Phys. Chem., 152* (2018), Nov., pp. 151-157
[11] Raza, J., *et al.*, Magnetohydrodynamic Flow of Nano Williamson Fluid Generated by Stretching Plate with Multiple Slips, *Multidiscipline Modeling in Materials and Structures, 15* (2019), 5, pp. 871-894
[12] Wakif, A., *et al.*, Numerical Study of the Onset of Convection in a Newtonian Nanofluid Layer with Spatially Uniform and Non-Uniform Internal Heating, *J. Nanofluids, 6* (2017), 1, pp. 136-148
[13] Lin, Y., *et al.*, MHD Pseudo-Plastic Nanofluid Unsteady Flow and Heat Transfer in a Finite Thin Film Over Stretching Surface with Internal Heat Generation, *Int. J. Heat Mass Transfer, 84* (2015), May, pp. 903-911
[14] Mahanthesh, B., *et al.*, Significance of Exponential Space- and Thermal-Dependent Heat Source Effects on Nanofluid Flow Due to Radially Elongated Disk with Coriolis and Lorentz Forces, *J. Therm. Anal. Calorim., 144* (2020), Nov., pp. 37-44
[15] Acharya, N., *et al.*, Framing the Effects of Solar Radiation on Magneto-Hydrodynamics Bioconvection Nanofluid Flow in Presence of Gyrotactic Microorganisms, *J. Mol. Liq., 222* (2016), Oct., pp. 28-37
[16] Mohammadi, K., Khorasanizadeh, H., A Review of Solar Radiation on Vertically Mounted Solar Surfaces and Proper Azimuth Angles in Six Iranian Major Cities, *Renew. Sustain. Energy Rev., 47* (2015), July, pp. 504-518
[17] Raza, J., *et al.*, Magnetohydrodynamic Flow of Molybdenum Disulfide Nanofluid in a Channel with Shape Effects, *Multidiscipline Modeling in Materials and Structures, 15* (2019), 4, pp. 737-757

[18] Hayat, T., *et al.*, Analysis of Non-Linear Radiative Stagnation Point Flow of Carreau Fluid with Homogeneous-Heterogeneous Reactions, *Microsyst. Technol., 25* (2019), 4, pp. 1243-1250
[19] Kuhn, S., Rudolf von Rohr, P., Experimental Study of Heat Flux in Mixed Convective Flow Over Solid Waves, *Exp. Fluids, 44* (2008), 6, pp. 973-984
[20] Jackson, J. D., *et al.*, Studies of Mixed Convection in Vertical Tubes, *Int. J. Heat. Fluid Flow., 10* (1989), 1, pp. 2-15
[21] Martinez-Suastegui, L., Trevino, C., Particle Image Velocimetry Measurements for Opposing Flow in a Vertical Channel with a Differential and Asymmetric Heating Condition, *Exp. Therm. Fluid Sci., 32* (2007), 1, pp. 262-275
[22] Hayat, T., *et al.*, Simultaneous Effects of Non-Linear Mixed Convection and Radiative Flow Due to Riga-Plate with Double Stratification, *J. Heat Transfer, 140* (2018), 10, 102008
[23] Sakiadis, B.C., Boundary-Layer Behavior on Continuous Solid Surfaces: I. Boundary-Layer Equations for Two-Dimensional and Axisymmetric Flow, *AIChE Journal, 7* (1961), 2628
[24] Vajravelu, K., Viscous Flow Over a Nonlinearly Stretching Sheet, *Appl. Math. Comput., 124* (2001), 3, pp. 281-288
[25] Ullah, I., *et al.*, Numerical Treatment of Melting Heat Transfer and Entropy Generation in Stagnation Point Flow of Hybrid Nanomaterials (SWCNT-MWCNT/Engine Oil), *Mod. Phys. Lett. B, 35* (2021), 6, 2150102
[26] Ismael, M.A., *et al.*, Effect of Driven Sidewalls on Mixed Convection in an Open Trapezoidal Cavity with a Channel, *J. Heat Transfer, 142* (2020), 8, 082601
[27] Lee, L. L., Boundary Layer Over a Thin Needle, *AIP Physics of Fluids, 10* (2014), 4, 1762194
[28] Fang, T., *et al.*, Boundary Layer Flow Over a stretching Sheet with Variable Thickness, *Appl. Math. Comput., 218* (2012), 13, pp. 7241-7252
[29] Hayat, T., *et al.*, Impact of Cattaneo-Christov Heat Flux in the Flow Over a Stretching Sheet with Variable Thickness, *AIP Advances, 5* (2015), 8, 087159
[30] Hayat, T., *et al.*, MHD Flow of Powell-Eyring Nanofluid over a Non-Linear Stretching Sheet with Variable Thickness, *Res. Phys., 7* (2017), pp. 189-196
[31] Javed, M., *et al.*, Analysis of Activation Energy and Melting Heat Transfer in MHD Flow with Chemical Reaction, *Eur. Phys. J. Plus, 134* (2019), 256
[32] Liao, S. J., On the Homotopy Analysis Method for Non-Linear Problems, *Appl. Math. Comput., 147* (2004), 2, pp. 499-513
[33] Malvandi, A., *et al.*, Stagnation Point Flow of a Nanofluid Toward an Exponentially Stretching Sheet with Nonuniform Heat Generation/Absorption, *J. Thermodynamics, 2013* (2013), 764827
[34] Hayat, T., *et al.*, MHD Mixed Convection Flow of Third Grade Liquid Subject to Non-Linear Thermal Radiation and Convective Condition, *Results Phys., 7* (2017), pp. 2804-2811
[35] Hayat, T., *et al.*, Double Stratified Flow of Nanofluid Subject to Temperature Based Thermal Conductivity and Heat Source, *Thermal Science, 24* (2020), 2B, pp. 1157-1171
[36] Hayat, T., *et al.*, Mixed Convective Radiative Flow of Vicoelastic Liquid Subject to Space Dependent Internal Heat Source and Chemical Reaction, *Thermal Science, 23* (2019), 6B, pp. 3843-3853
[37] Hayat, T., *et al.*, Flow of Chemically Reactive Magneto Cross Nanoliquid with Temperature-Dependent Conductivity, *Appl. Nanosci., 8* (2018), 6, pp. 1453-1460
[38] Qiang, X., *et al.*, Numerical Approximation of Fractional-Order Volterra Integrodifferential Equation. *Journal of Function Spaces, 2020* (2020), ID 8875792
[39] Chu, Y. M., *et al.*, Numerical and Computer Simulations of Cross-Flow in the Streamwise Direction through a Moving Surface Comprising the Significant Impacts of Viscous Dissipation and Magnetic Fields: Stability Analysis and Dual Solutions, *Mathematical Problems in Engineering, 2020* (2020), ID 8542396
[40] Abd El Salam, M. A., *et al.*, Matrix Computational Collocation Approach Based on Rational Chebyshev Functions for Nonlinear Differential Equations, *Advances in Difference Equations, 2021* (2021), 331
[41] Chu, Y. M., *et al.*, Analysis of Fractional Multi-Dimensional Navier-Stokes Equation, *Advances in Difference Equations, 2021* (2021), 91
[42] Chu, Y. M., *et al.*, Enhancement in Thermal Energy and Solute Particles Using Hybrid Nanoparticles by Engaging Activation Energy and Chemical Reaction over a Parabolic Surface via Finite Element Approach, *Fractal and Fractional, 5* (2021) 3, 119

[43] Chen, S. B., *et al.,* The Effect of Market Confidence on a Financial System from the Perspective of Fractional Calculus: Numerical Investigation and Circuit Realization, *Chaos, Solitons & Fractals, 140* (2020), Nov., 110223
[44] Zhao, T. H., *et al.,* Artificial Neural Networking (ANN) Analysis for Heat and Entropy Generation in Flow of Non-Newtonian Fluid between Two Rotating Disks, *Mathematical Methods in the Applied Sciences,* On-line first, https://doi.org/10.1002/mma.7310, 2021
[45] Ullah, I., Activation Energy with Exothermic/Endothermic Reaction and Coriolis Force Effects on Magnetized Nanomaterials Flow through Darcy-Forchheimer Porous Space with Variable Features, *Waves in Random and Complex Media,* On-line first, https://doi.org/10.1080/17455030.2021.2023779, 2022

Paper submitted: October 15, 2020
Paper revised: March 5, 2021
Paper accepted: March 20, 2021